Research Square

Preprints are preliminary reports that have not undergone peer review.
They should not be considered conclusive, used to inform clinical practice,
or referenced by the media as validated information.

Improvement of dielectric and structural characteristics of Nanofiller (Ba0.92Sr0.08)TiO3 Ceramics combined with epoxy as composites for dielectric purposes

Mahmoud Rihan
Qena University
Gehad Mohamed Elsaleh Rashwan
gmraswan10@gmail.com

Luxor University
Loai Nasrat
Aswan University
Abdelhameid Ghazzaly
Qena University
Massaud Mostafa
Qena University
Gehad Mohamed Elsaleh Rashwan
Luxor University

Research Article

Keywords: Barium strontium titanate, Epoxy, Polymer–ceramic composite

Posted Date: November 13th, 2026

DOI: https://doi.org/10.21203/rs.3.rs-11085371/v1

License: This work is licensed under a Creative Commons Attribution 4.0 International License.
Read Full License

Additional Declarations: No competing interests reported.

Improvement of dielectric and structural characteristics of Nanofiller ($Ba_{0.92}Sr_{0.08}$)TiO_3 Ceramics combined with epoxy as composites for dielectric purposes.

Mahmoud Rihan [1], G.M. Rashwan [*2,4], Loai S. Nasrat [3] , Abdelhameid Ghazzaly [1], and Massaud. Mostafa [*2]

[1] Electrical Engineering Department, Faculty of Engineering, South Valley University, Qena 83521, Egypt.
[2] Physics Department, Faculty of Science, South Valley University, Qena 83523, Egypt.
[3] Electrical Engineering Department, Faculty of Engineering, Aswan University, Aswan, Egypt.
[4] Physics Department, Faculty of Science, luxor university, Luxor 85951, Egypt.

Abstract

Polymer Nano composites were created by reinforcing epoxy with barium titanate ($B_{0.92}$ $S_{0.08}$) TiO_3, boasting high dielectric strength. These composites showcased significant alterations in their dielectric capabilities, influenced by time, temperature, and concentration. The research delved into epoxy resin composites, exploring how the ratio of BST nanoparticles affected the dielectric strength concerning the epoxy aspect ratio. Epoxy was combined with nano filler titanate ($B_{0.92}$ $S_{0.08}$) TiO_3 Ceramics at various BST to epoxy ratios of 0%, 2.5%, 5%, 7%, and 100%, with the mixture left to cure in an oven at temperatures of 40°C, 50°C, 60°C, and 80°C for durations ranging from 10 to 50 minutes. The temperature was consistently set at 50°C, while curing times varied from 10 to 50 minutes. The study also delved into the mechanical bonding mechanisms between BST and epoxy polymer. Techniques such as Scanning Electron Microscopy (SEM) and Transmission Electron Microscopy (TEM) were employed to study delaminated layers, inspect fracture surfaces, and assess structural features and dielectric strength. Discussions revolved around the impacts of concentration, particle size, and BST filler on the dielectric properties of BST/polymer composites. Artificial Neural Networks, known as ANNs, mimic the intricate workings of the human brain to delve into the realms of ceramic/polymer composites' dielectric constants and the crafting of BST/polymer composites. Delving deeper, the enhancement of dielectric constants in BST/polymer composites is succinctly outlined. A novel theoretical model focusing on dielectric constants, drawn from our prior research endeavors, is presented. Furthermore, the impacts of various factors on the dielectric constants of these composites are explored, aiding in the forecast of their dielectric constants. This discussion holds significant theoretical and research implications for future endeavors.

Keywords: Barium strontium titanate, Epoxy, Polymer–ceramic composite.

* **Corresponding author:** Massaud. Mostafa **E-mail address**: masoud.mostafa@sci.svu.edu.eg

G.M.Rashwan (Gehad Mohamed) **E-mail address** gmrashwan@GMail.com

1.Introduction

The use of polymeric materials in engineering applications has grown dramatically. Because of their high adhesive qualities, powerful cross-linking networks, outstanding dimensional stability [1], and superior chemical and thermal resistance, thermoset polymers are especially well-liked in industrial settings. Nevertheless, they frequently lack the required strength and stiffness despite their advantageous qualities, such as low density, light weight, resistance to corrosion, and design flexibility. Reinforcing these polymers with high-strength, lightweight materials like glass and carbon fibers fills this gap. Polymer composites are useful in many structural and tribological applications because of these benefits [2]. Epoxy has special characteristics among polymers because it is inexpensive to produce and simple to prepare [3]. Epoxy resin is a thermosetting polymer that is renowned for its exceptional resilience and mechanical qualities. The term "epoxy" is frequently used to describe the main ingredients of epoxy resins or the final product after curing. Monomers with at least two epoxide groups give rise to this family of thermoset polymers. Curatives can be used to cross-link or polymerize them into a three-dimensional network. A variety of curatives or hardeners, such as polyfunctional acids, amines, phenols, thiols, alcohols, and anhydrides, are available for curing, whether at room temperature or at higher temperatures [4–8]. Being one of the most powerful chemical adhesives on sale, epoxy finds extensive use in adhesive applications. It is widely utilized in the automotive and aerospace sectors. Particularly noteworthy are solvent-free epoxy adhesives' exceptional durability, chemical and heat resistance, and water resistance. Because they offer a strong, protective covering with remarkable hardness, epoxy-based coatings are often used on metal substrates where good performance is crucial [9–11]. Because of its excellent dielectric qualities, corrosion resistance, low shrinkage while curing, high stiffness and strength [12], chemical resistance, and superior thermal properties [13], epoxy is the most important family of thermosetting resins for a variety of engineering applications. Researchers have developed a range of nanostructured materials composed of polymers, inorganic substances, and composites. Support materials such as iron oxide (Fe2O3), magnesium oxide, zinc oxide (ZnO), titanium dioxide, gold, and silver are used in these structures. Even in harsh environments, magnesium

oxide (MgO) is renowned for its chemical and thermal stability. It also has exceptional biocompatibility, dissolving into soluble, non-toxic Mg+2 ions [11]. Ferroelectric barium titanate (BaTiO3) is distinguished by its positive temperature coefficient, low dissipation factor, and high dielectric constant [14–16]. Because of its high dielectric constant, superior thermal stability, and enhanced properties when doped with other materials, barium strontium titanate (BST) is a better choice for a dielectric material [17]. A perovskite structure known as $(Ba_{1-x}Sr_x)TiO_3$, or BST, can develop in this material when Ba ions are swapped out for Sr ions. The ferroelectric/paraelectric transition temperature can be adjusted for purposes because the Curie temperature of BST falls linearly with increasing Sr concentration. Consequently, the Ba: Sr ratio can have a significant impact on the electrical and optical characteristics of BST. Because of its strong dielectric permittivity, barium strontium titanate has garnered a lot of attention from scientists and engineers [18].

Computational models known as artificial neural networks (ANNs) are modeled after the composition and operations of the human brain. They use a connectionist computation approach to process information and are made up of interconnected clusters of artificial neurons. Because ANNs can learn and generalize from data, they are frequently utilized for a variety of applications, such as pattern recognition, classification, and prediction [19]. A feedforward neural network, a kind of ANN in which node-to-node connections do not create cycles, was employed in this investigation [20]. When the objective of supervised learning tasks is to predict an output based on a given input, this model performs especially well [21]. The following are the main benefits of ANNs: Adaptability: ANNs are flexible for a range of applications because they can adjust to changing circumstances and learn from the data they process [19,22]. Nonlinear Processing: Conventional linear models are unable to capture the intricate, nonlinear interactions between input and output variables that artificial neural networks (ANNs) can [23,24],.Robustness: ANNs are appropriate for real-world applications where data quality varies because they can manage noisy and incomplete data well [20,25].Parallel Processing: ANNs' structure allows them to execute several tasks at once, boosting computing efficiency [19,24].

The purpose of this study is to examine the effects of nano $(Ba_{0.92}\ Sr_{0.08})TiO_3$ particles on the fracture behavior of epoxy composites created via mold casting. The mechanical bonding

procedures between epoxy polymer and BST are also described. Characterizing delaminated layers involves analyzing their fracture surfaces, characterizing their structural properties, and determining their dielectric strength using analytical methods such as Scanning Electron Microscopy (SEM) and Transmission Electron Microscopy (TEM). The flexibility and capacity to represent nonlinear interactions of the feed forward neural network were then essential in precisely forecasting the dielectric strength of unmanufactured epoxy nanocomposites depending on filler content, temperature, and time.

2. Experimental

2.1. Materials

All the samples were made using materials that might be purchased commercially. The present study specifically used a cycloaliphatic epoxy resin (6105, DOW Chemicals, USA) in conjunction with methyl-hexahydrophthalic anhydride (MHHPA, Shanghai Li Yi Science & Technology Development Co. Ltd., China) as a hardener, barium acetate (ACS reagent grade, 99%, Merck, Germany), strontium acetate (ACS reagent grade, 99.9%, Sigma Aldrich, USA), and titanium (IV) isopropoxide (ACS reagent grade, 99.9%, Sigma Aldrich, USA).

2.2. Barium strontium titanate preparation.

As precursors for barium, strontium, and titanium, respectively, the (Ba0.92 Sr0.08)TiO3 nanopowder was created using barium acetate (ACS reagent grade, 99%, Merck, Germany), strontium acetate (ACS reagent grade, 99.9%, Sigma Aldrich, USA), and titanium (IV) isopropoxide (ACS reagent grade, 99.9%, Sigma Aldrich, USA). Titanium (IV) isopropoxide was stabilized using ethanol (99+%, Merck, Germany) and acetic acid (glacial, 99 to 100% EMPLURA, Merck, Germany) as a solvent. Continuous magnetic stirring at 300 rpm for 30 minutes was used to dissolve stoichiometric amounts of barium acetate (0.04 mol) and strontium acetate (0.026 mol) powders in 10 and 12 mL of heated glacial acetic acid, respectively. After that, the two solutions were combined and agitated for 30 minutes at 300 rpm. At room temperature, titanium (IV) isopropoxide (0.066 mol) was mixed with 2 to 5 mL of ethanol to create a distinct solution. With the aid of a burette, drops of the Ba–Sr solution was added to the Ti solution as it was created. By adding buffering agents, the pH of the solution was kept between 3.5 and 5. A thick, white-colored gel formed because of refluxing. After cooling the produced gel to 5 °C, deionized water was added, and the mixture was magnetically agitated for 60 minutes. Amorphous ($B_{0.92}\,S_{0.08}$) TiO_3 powder was formed when the solution was dried at 100 °C and heated to 200 °C for two hours to fully separate the water. After that, the amorphous powder was calcined in a muffle furnace at 600, 750, and 850 °C, respectively, to crystallize it. A process diagram illustrating the manufacture of nanocrystalline BST powder is shown in Fig. 1 [26].

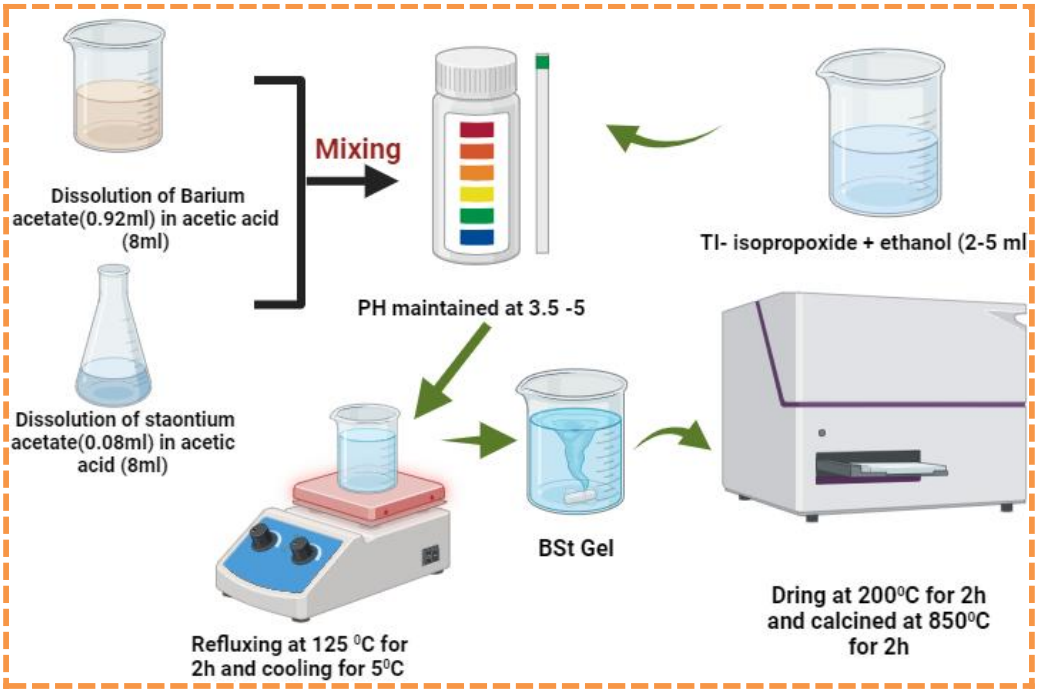


Figure1: Experimental procedure for preparation of ($B_{0.92}$ $S_{0.08}$) TiO_3 ceramic material.

2.3. ($B_{0.92}$ $S_{0.08}$) TiO_3 with epoxy preparation.

To examine the impact of (B $S_{0.08}T_{0.92}$) fillers on the dielectric characteristics, a sample of ($B_{0.92}$ $S_{0.08}$) TiO_3 with epoxy composites was created. For the investigations, Huntsman's bisphenol An epoxy resin (CT 5531 CI) and hardener (HT 903 CI) are utilized. Because of its great mechanical strength and superior heat-shock resistance, this type of epoxy resin is typically used in high-voltage electrical equipment, including as switch devices, bushings, and GIS spacers. A homogenous mixture of 100 parts by weight of CT 5531 CI resin and 38 parts by weight of HT 903 CI hardener is required to process a sample using this epoxy resin and hardener. Regarding the fillers, solid stat reaction was prepared using ($B_{0.92}$ $S_{0.08}$) TiO_3 particles.

The surfaces of ($B_{0.92}$ $S_{0.08}$) TiO_3 particles were modified using a silane coupling agent to get around this aggregation issue. The first step involved adding the modified dry (B $S_{0.08}T_{0.92}$)O_3 particles to an ethanol solution and ultrasonically mixing them for 60 seconds. To avoid sedimentation, the ethanol solution doped with ($B_{0.92}$ $S_{0.08}$) TiO_3 particles is then added to the high viscosity pure epoxy first [27]. To get a good dispersion, the mixture is agitated in a mixer for an hour. Then, after a few minutes of continuous mixing in the mixer, a certain amount of hardener is added to the mixture and poured into the mold. After that, the mold is placed in an oven to cure; the temperature and duration of this process were discussed in this work [28]. As illustrated in figure 2, a vacuum system (10–2 bar) is required at each stage of the procedure in

order to eliminate bubbles from the samples. Air bubbles can function as flaws and have a big impact on the epoxy composites' dielectric qualities. Air bubbles may become trapped in the substance during sample preparation, particularly when mixing. Therefore, before the curing process, the mold containing the composite material must be degassed until the air bubbles completely stop escaping the material.

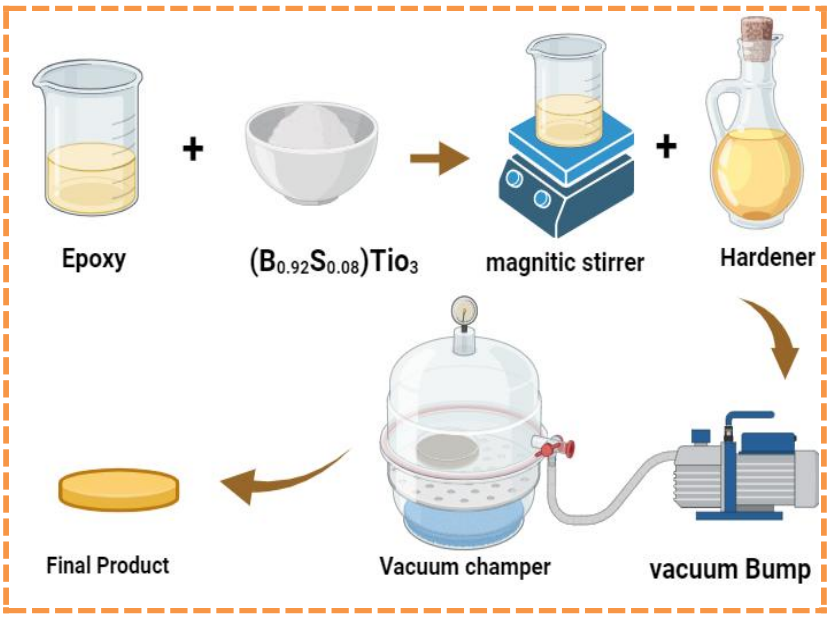


Figure 2: Experimental technique for preparation and curing of Epoxy Nano composite.

2.4 Neural network's Methodology

Different input parameters were used in two sets of studies. Temperature (from 40°C to 80°C) and filler concentration (from 0% to 10%) were the input variables in the first set. Time (from 10 to 50 minutes) and filler concentration (from 0% to 10%) were the input variables in the second set. The measured dielectric strength values for these input combinations made up the output dataset. To increase the effectiveness and precision of the ANN training procedure, the datasets were normalized using MATLAB's map minmax function [19,21]. The ANN for each set was constructed with a feedforward network architecture, comprising two hidden layers with 10 neurons each [21,22] . The network configuration and training parameters were set as follows:

- Training, validation, and testing data were divided in the ratio of 70:15:15.
- The training was set to continue until a performance goal of 1×10^{-6} was achieved, or until the minimum gradient of 1×10^{-7} was reached.
- The learning rate was set at 0.01, with a maximum of 2000 epochs per training session, and a maximum of 6 validation failures allowed.

2.5 Training and Performance

The ANN was trained iteratively, with the prediction errors being checked until the predetermined conditions were satisfied. The performance metric employed was mean squared error (MSE) [24] . The training cycle went on until either 10,000 epochs were attained or all percentage errors were less than 0.9%. The ANN showed excellent accuracy in predicting dielectric strength for the first set of experiments (temperature and filler content). The percentage errors for individual forecasts were kept below the designated cutoff of 0.9%, and the total mean squared error was kept to a minimum [24]. For the second set of experiments (time and filler concentration), similar high accuracy was achieved, demonstrating the robustness of the ANN model in predicting dielectric strength under different conditions [29].

3- Characterization

One of the most important methods for describing the structural characteristics of CNPs is the X-ray diffraction (XRD) pattern. A diffractometer of the type of Cu Kα radiation (λ = 1.54 A°) was used to perform X-ray diffraction measurements at room temperature. The generator was operating at 10 kV and 30 mA of current. High-resolution scanning electron microscopy (SEM, JEOL JEM-2100) (Japan) and transmission electron microscopy (TEM, JOUL, JSM-1010, Japan) were utilized to analyze the surface morphology of the composite bricks. Data were gathered at a scanning rate of 2°/min for 2θ between 0 and 40.

4- Result and Discussion

4.1. X-ray Diffraction

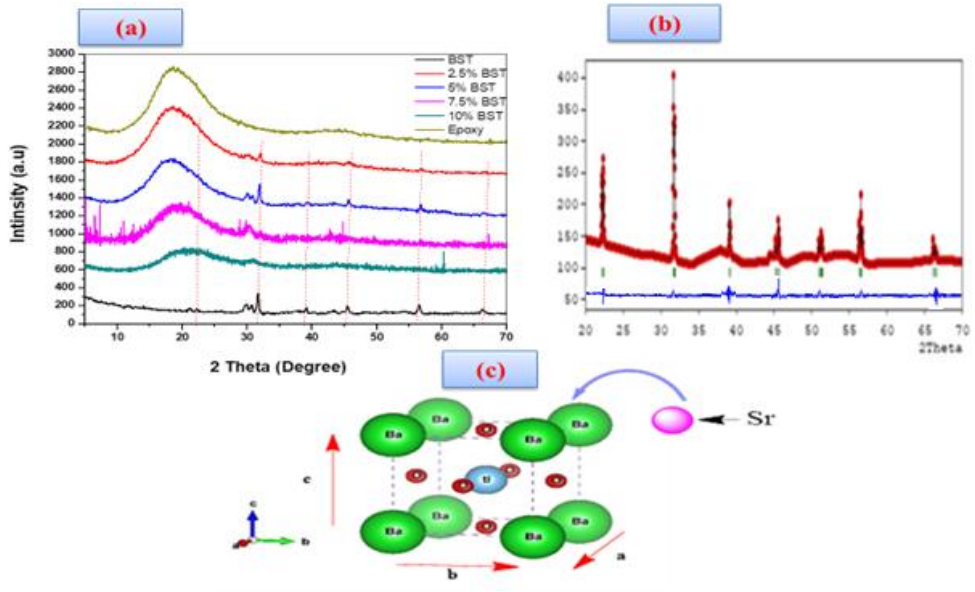


Figure 3: XRD spectra of $(B_{0.92}\ S_{0.08})\ TiO_3$ nano powder, pure Epoxy and composite of them(a), Least-squares structure refinements for $(B_{0.92}\ S_{0.08})\ TiO_3$ NPs (b), VESTA (Visualization for Electronics and Structural Analysis) program for The crystal structure of $(Ba_{0.92}\ Sr_{0.08})TiO_3$ NPs (c).

Figure 3 displays the XRD spectra of every sample that was analyzed, including the pure epoxy, pure ($B_{0.92}$ $S_{0.08}$) TiO_3 nanopowder, and their composite. Figure 3 displays the final calcined powder's X-ray diffraction pattern at 850°C BST. Diffraction angles 2θ=22.43º, 31.9º, 39.33º, 45.72º, 51.47º, 56.81º, and 66.63º show intense peaks. Every peak match JCPDS card number 440093 and is associated with the tetragonal phase of BST. The (100), (110), (111), (002), (210), (211), and (202) planes are the indexes for the diffraction peaks. Furthermore, the BST sample's tetragonal structure is confirmed by the peak splitting at diffraction angles 45.72º and 66.63º [30]. The FULLPROF Rietveld-type program was used to model the refinements of the least-squares structure. The results showed the expected R-fac tor (Rexp) = 29.82, the weighted pattern R-factor (Rwp) = 45, and the traditional Rietveld R-factors Rp = 25. A plot of the observed, computed, and difference profiles for the last Rietveld refinement of biogenically produced ($B_{0.92}$ $S_{0.08}$) TiO_3 nanoparticles (NPS) is shown in Figure (3-b). The agreement between the data and the model during the Rietveld refinements is shown by the blue line in Figure (3-b). For the tetragonal structure, the space group P4mm was taken into consideration when doing the study. Numerous XRD data characteristics, including refinement parameters like occupancy, atomic functional position, crystal system, space group, and cell parameter, were fitted using a pseudo-Voigt function [31] .The final Rietveld refinement parameters were used in the standardization of the crystal structure and fractional coordinates modeled by the VESTA (Visualization for Electronics and Structural Analysis) program [32], as shown in Figure (3-c). The crystal structure of ($Ba_{0.92}$ $Sr_{0.08}$)TiO_3 NPs was confirmed to be tetragonal, corresponding to the space group P4mm. The tetragonal unit cell has three lattice parameters, a =b = 3.994, , and c= 4.008, with a c/a ratio of 1.003 and α = β = γ= 90 º, Moreover the lattice parameters positions and cell volume shown in table 1.In Figure (3-b), the ($B_{0.92}$ $S_{0.08}$) TiO_3 structural model is schematically represented using the final Rietveld refinement parameters. Two interpenetrating tetragonal sublattices make up the structure [30]. The broad peak in the XRD pattern, which spans from 12° to 30°, indicates that pure epoxy (P) has an amorphous structure. This broad peak, associated with the amorphous structure of the epoxy, reduces with the addition of ($B_{0.92}$ $S_{0.08}$) TiO_3 nanoparticles. Furthermore, the peaks corresponding to the ($B_{0.92}$ $S_{0.08}$) TiO_3 nanoparticles become increasingly apparent as the nanoparticle filler content increases.

Table 1: Final Rietveld refinement parameter of Tetragonal ($Ba_{0.92}$ $Sr_{0.08}$)TiO_3 NPs.

Compound	Space group	a(A°)	b(A°)	c(A°)	α =β = γ	C/ a	Cell volume (A°)	Atom	x	Y	Z
($Ba_{0.92}$ $Sr_{0.08}$)TiO_3	P4mm	3.994	3.994	4.003	90º	1.003	63.855	Ba	0	0	0
								Sr	0	0	0
								Ti	0.5	0.5	0.486
								O	0.5		0.162

4.2. Surface morphology.

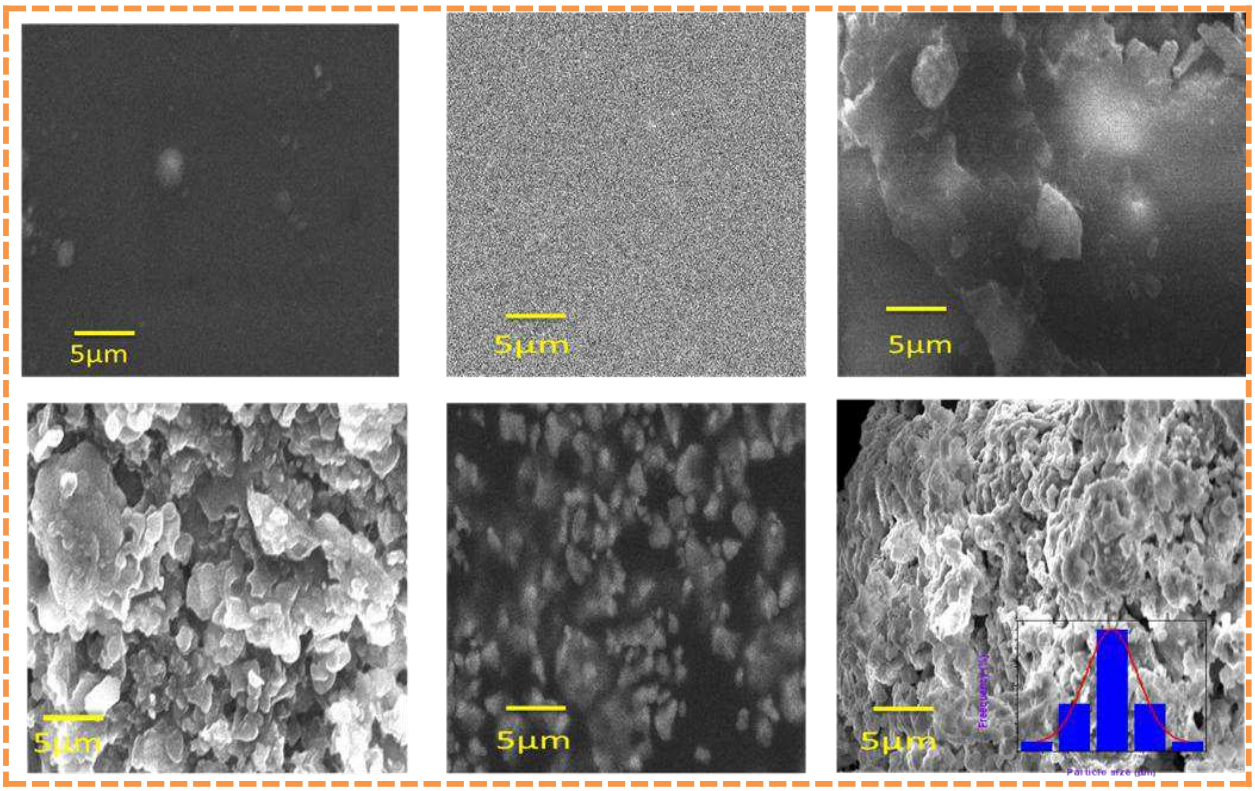


Figure 4: SEM of pure epoxy (a) BST2.5, (b) BST5, (c) BST7.5, (d) and BST10 (e) and pure ($B_{0.92}$ $S_{0.08}$) TiO_3 nano powder (g).

Figure 4 shows images from the SEM of every sample that was analyzed, including composites of BST2.5 (b), BST5 (c), BST7.5 (d), and BST10 (e), as well as pure epoxy (a) and pure ($B_{0.92}$ $S_{0.08}$) TiO_3 nanopowder (g).Achieving a uniform dispersion of nanofillers within the polymer is one of the main challenges in the production of nanocomposites. The thermal and mechanical properties of polymers can be negatively impacted by nanoparticle agglomeration, and the probability of agglomeration rises with increasing filler loading. Furthermore, the BST nanoparticles in the nanocomposites need to be evenly distributed. Figure 4 displays the distribution of BST nanoparticles in polymer-based matrices to examine morphological characteristics.

The mixing procedures during preparation were carefully carried out to achieve equal dispersion of nanofillers in the samples, as evidenced by the various architectures of the created nanocomposites and the physical characteristics of the nanoparticles and polymers utilized [33]. Figure (4-g) illustrates the cauliflower-like structure of the ($B_{0.92}$ $S_{0.08}$) TiO_3 nanoparticles, which are found in very small numbers and spaced widely apart. Clusters and finely dispersed nanoparticles coexist, as evidenced by the increasing density of BST inclusions with increasing

filler concentration. Figure (4-c) also shows some microcracks and voids, despite the fillers being evenly mixed in the BST5 [34] .

4.3. Transmission Electron Microscope

The BT nanoparticles that were received are comparatively homogeneous in size, with a range of 10–15 nm. The morphologies of the $(Ba_{0.092}\ Sr_{0.08})TiO_3$ surface were thus further investigated using transmission electron microscopy. Following modification, a sizable number of $(Ba_{0.092}\ Sr_{0.08})TiO_3$ nanoparticles with a consistent size of 10 nm are homogeneously [35] .

Greater agglomeration took place in these circumstances, as evidenced by the bigger area and more noticeable black dots as shown in figure 5. This could be because, although being lipophilic, $(Ba_{0.092}\ Sr_{0.08})TiO_3$ does not readily disperse in some situations due to its tiny particle size (around 10-15 nm) and high surface energy. Nevertheless, agglomeration was exacerbated by the 30-minute ultrasonic treatment [36]. The composite's compressive strength was increased when the $(Ba_{0.092}\ Sr_{0.08})TiO_3$ value was low and no ultrasonic treatment was used; however, when agglomeration increased at greater concentrations, the compressive strength decreased [37] .

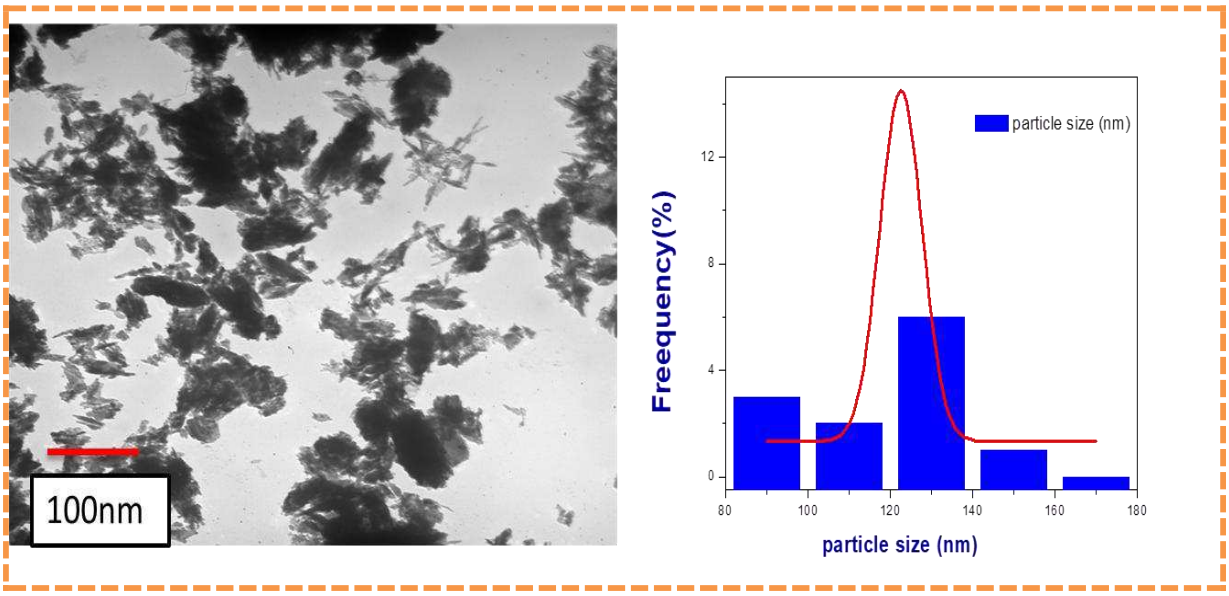


Figure 5: Transmission Electron microscope of $(Ba_{0.092}\ Sr_{0.08})TiO_3$ Nanoparticle .

2.5. Dielectric Analysis the ANN models.

An example prediction was performed for new input scenarios. For the first set of experiments, with a time of 45 minutes and a filler concentration of 4%, the predicted dielectric strength was 55.23 kV/mm. For the second set of experiments, with a temperature of 45°C and a filler concentration of 4%, the predicted dielectric strength was 38.35 kV/mm.

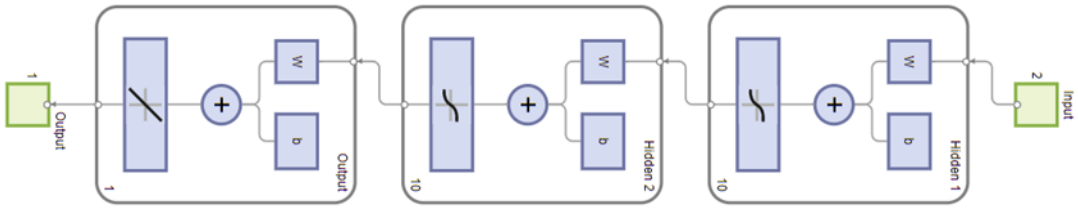


Figure 6: Structure of the Feedforward Neural Network

Figure 6 illustrates the architecture of the feedforward neural network used in the study, showing the input layer, hidden layers, and output layer. It was generated using MATLAB's view(net) function.

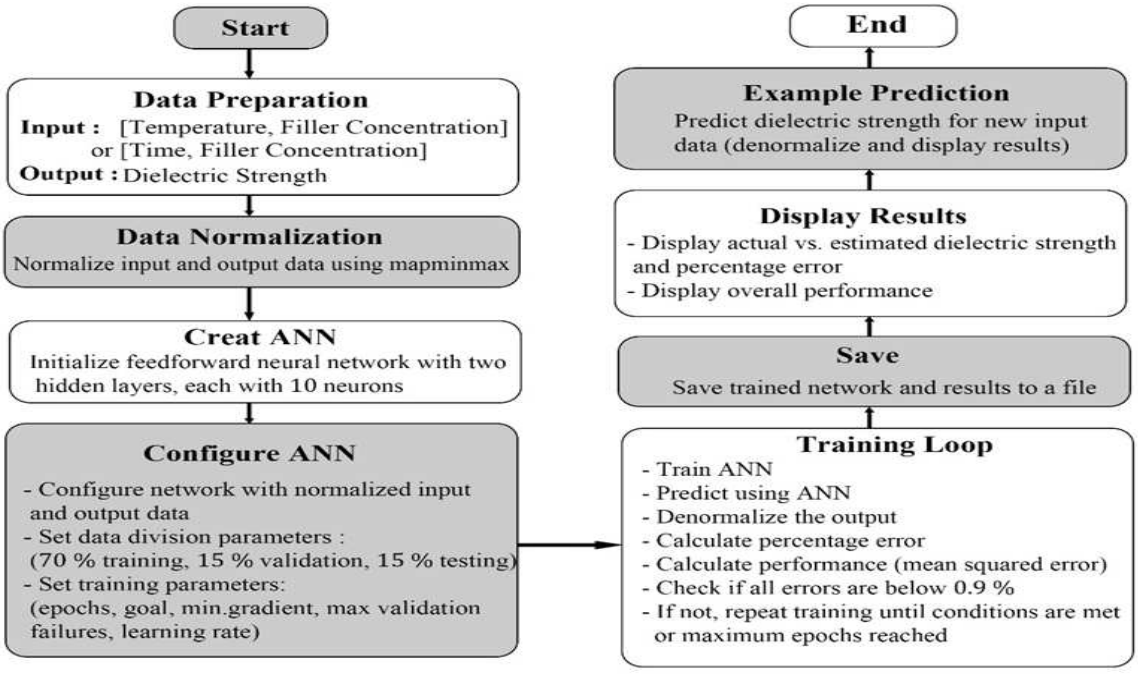


Figure 7: Detailed Flowchart of ANN Process

Figure 7 provides a detailed flowchart of the ANN process, including steps such as data preparation, normalization, ANN creation, configuration, training loop, saving results, displaying results, and example prediction.

The best results obtained for the ANN models as mentioned in table 1:

Table 1: First Set of Experiments (Time and Filler Concentration)

Time (min)	Filler Concentration (%)	Actual Dielectric Strength (kV/mm)	Estimated Dielectric Strength (kV/mm)	Percent Error (%)
10.00	0.00	36.00	36.00	0.01
10.00	2.50	44.00	44.00	0.00
10.00	5.00	48.00	48.01	0.02
10.00	7.50	58.00	57.97	0.05
10.00	10.00	81.00	81.09	0.11
20.00	0.00	48.00	48.00	0.01
20.00	2.50	47.00	47.04	0.08
20.00	5.00	56.00	56.00	0.00
20.00	7.50	65.00	65.00	0.01
20.00	10.00	85.00	85.02	0.02
30.00	0.00	44.00	44.00	0.01
30.00	2.50	46.00	46.00	0.01
30.00	5.00	61.00	61.00	0.00
30.00	7.50	72.00	71.99	0.02
30.00	10.00	76.00	75.99	0.01
40.00	0.00	41.00	40.99	0.02
40.00	2.50	44.00	44.00	0.00
40.00	5.00	60.00	60.01	0.02
40.00	7.50	69.00	68.75	0.36
40.00	10.00	70.00	69.68	0.45
50.00	0.00	35.00	35.00	0.00
50.00	2.50	40.00	39.98	0.06
50.00	5.00	55.00	55.03	0.05
50.00	7.50	60.00	59.96	0.06
50.00	10.00	63.00	63.05	0.08

The ANN model for the first set of experiments (time and filler concentration) demonstrated excellent performance with an overall mean squared error of 0.000012. The percentage error for

the predictions was consistently below 0.9%, indicating the high accuracy and reliability of the model.

Table 2:Second Set of Experiments (Temperature and Filler Concentration)

Temperature (°C)	Filler Concentration (%)	Actual Dielectric Strength (kV/mm)	Estimated Dielectric Strength (kV/mm)	Percent Error (%)
40.00	0.00	14.00	14.00	0.02
40.00	2.50	34.00	34.00	0.00
40.00	5.00	37.00	37.08	0.21
40.00	7.50	46.00	46.00	0.00
40.00	10.00	70.00	70.00	0.00
50.00	0.00	36.00	36.00	0.01
50.00	2.50	44.00	44.00	0.00
50.00	5.00	48.00	48.00	0.01
50.00	7.50	58.00	58.00	0.00
50.00	10.00	81.00	81.00	0.00
60.00	0.00	43.00	43.00	0.00
60.00	2.50	53.00	52.96	0.08
60.00	5.00	56.00	55.99	0.01
60.00	7.50	66.00	65.53	0.71
60.00	10.00	85.00	85.21	0.24
70.00	0.00	46.00	45.97	0.06
70.00	2.50	65.00	65.00	0.00
70.00	5.00	58.00	57.99	0.01
70.00	7.50	69.00	69.00	0.00
70.00	10.00	80.00	80.00	0.00
80.00	0.00	37.00	37.02	0.05
80.00	2.50	46.00	46.00	0.00
80.00	5.00	50.00	50.00	0.00
80.00	7.50	61.00	61.00	0.00
80.00	10.00	70.00	70.00	0.00

The ANN model for the second set of experiments (temperature and filler concentration) also demonstrated excellent performance with an overall mean squared error of 0.000009 as mentioned in table 2. The model achieved a perfect or near-perfect fit for most data points, with percentage errors consistently below 0.9%, underscoring its accuracy and reliability.

Table 3: Dielectric strength (KV/mm) at 10 min for different temperatures.

Filler	40°C			50°C			60°C			70°C			80°C		
	Actual	Predicted	Error	Actual	Predicted	Error	Actual	Predicted	Error	Actual	Predicted	Error	Actual	Predicted	Error
Zero%	14	14	0	36	36	0.01	43	43	0.00	46	45.97	0.06	37	37.02	0.05
2.50%	34	34	0.00	44	44	0.00	53	52.96	0.08	65	65	0.00	46	46	0.00
5%	37	37	0	48	48	0.01	56	55.99	0.01	58	57.99	0.01	50	50	0.00
7.50%	46	46	0.00	58	58	0.00	66	65.53	0.71	69	69	0.00	61	61	0.00
10%	70	70	0.00	81	81	0.00	85	85.21	0.24	80	80	0.00	70	70	0.00

Table 4: Dielectric strength (KV/mm) at 50°C for different times.

Filler	10min			20min			30min			40min			50min		
	Actual	Predicted	Error	Actual	Predicted	Error	Actual	Predicted	Error	Actual	Predicted	Error	Actual	Predicted	Error
Zero%	36	36	0.01	48	48	0.01	44	44	0.01	41	40.99	0.02	35	35	0.00
2.50%	44	44	0.00	47	47.04	0.08	46	46	0.01	44	44	0.00	40	39.98	0.06
5%	48	48.01	0.02	56	56	0.00	61	61	0.00	60	60.01	0.02	55	55.03	0.05
7.50%	58	57.97	0.05	65	65	0.01	72	71.99	0.02	69	68.75	0.36	60	59.96	0.06
10%	81	81.09	0.11	85	85.02	0.02	76	75.99	0.01	70	69.68	0.45	63	63.05	0.08

Table 3 shows the actual dielectric strength (KV/mm) results at 10 minutes for different filler concentrations (0, 2, 5, 7.5, and 10) at different temperatures (40, 50, 60, 70, and 80). The ANN model's calculated values and the actual measured values are compared as well in the table. The results show that dielectric strength values obviously increase with increasing filler concentration and temperature. The ANN model may be able to predict the dielectric strength values with accuracy for other values that were not tested in practice. For instance, it was measured at 4% filler concentration, with the expected dielectric strength being 38.35 kV/mm, the overall mean squared error being 0.000009, the training performance being 0.000000, the validation performance being 0.000045 and the test performance being 0.000009, with the new input temperature being 45.00°C.

The actual dielectric strength (KV/mm) findings at 50°C for various filler concentrations (0, 2, 5, 7.5, and 10) at various times (10, 20, 30, 40, and 50 minutes) are displayed in Table 4. The table also compares the calculated values from the ANN model with the actual measured values. The results obtained demonstrate that dielectric strength values clearly rise as filler concentration and time increase. For other values that were not tested in practice, the ANN model could be able to predict with confidence the dielectric strength values. For example, the dielectric strength was expected to be 55.23 kV/mm at a filler concentration of 4%, the training performance was 0.000001, the validation performance was 0.000000, and the test performance was 0.000069; the new input temperature was set at 45.00 minutes. The overall mean squared error was 0.000012.

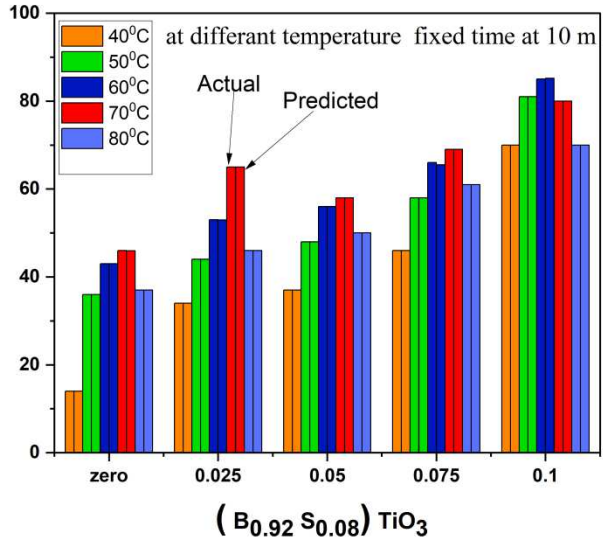


Figure 8: Comparison between the actual and predicted dielectric strength (KV/mm) values for different temperatures at fixed time (10 min) .

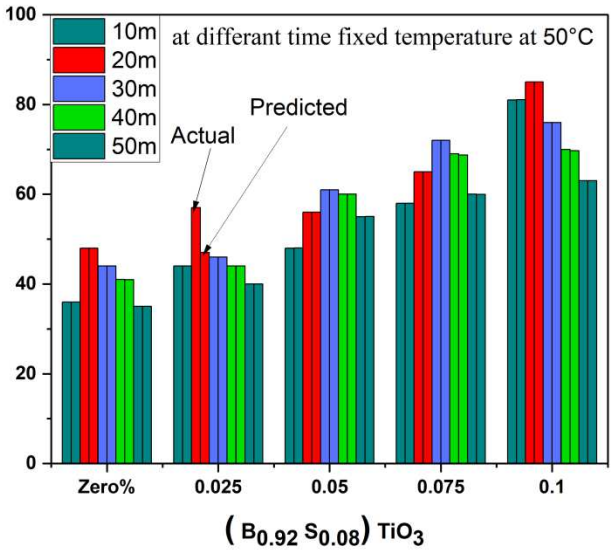


Figure 9 : Comparison between the actual and predicted dielectric strength (KV/mm) values for different times at fixed temperature (50 ◦C) .

Figure 8 shows a comparison of actual and predicted dielectric strength in (KV/mm) values for nano filler molds cured in an oven at 40, 50, 60, and 80 ◦C for 10 minutes. Figure 9 shows the temperature being fixed at 50°C for varying times (10, 20, 30, 40, 50 minutes). Overall, there is high agreement between actual and anticipated dielectric strength values. The dielectric strength values gradually rose over time at fixed temperatures. Similarly, it gradually grew with rising temperatures at a predetermined time. Higher mold temperatures typically speed up the curing process of the binder or ceramic matrix into which the nanofillers are disseminated. This is because heat supplies the activation energy that allows chemical reactions (such as cross-linking) to proceed more quickly. There is usually an ideal temperature range for curing. Too low a temperature might cause inadequate curing, which results in weaker, less dense materials. The mold temperature has a direct impact on the final degree of cure, or the intensity of the chemical reactions. More cure generally results in improved mechanical and thermal qualities. An adequate mold temperature during curing helps to achieve excellent bonding between the nanofillers and the matrix, as well as inside the matrix itself. This can greatly improve mechanical qualities like tensile strength, flexural strength, elastic modulus, and fracture toughness. Inadequate curing owing to low mold temperature might result in brittle materials.

Conclusion:

This study successfully investigated the dielectric and structural properties of epoxy composites reinforced with nano $(Ba_{0.92}\ Sr_{0.08})TiO_3$(BST) ceramic fillers for dielectric applications. The research highlighted the significant influence of time, temperature, and filler concentration on the dielectric strength of the prepared polymer nanocomposites.

The $(Ba_{0.92}\ Sr_{0.08})TiO_3$ Nano powder was synthesized using a sol-gel method, and X-ray diffraction (XRD) analysis confirmed its tetragonal crystal structure, consistent with JCPDS card number 440093. The SEM images revealed the cauliflower-like structure of the BST nanoparticles and demonstrated that careful mixing procedures resulted in an even dispersion of nanofillers within the epoxy matrix, despite some observed microcracks and voids at higher concentrations. TEM analysis further showed that the received BT nanoparticles were relatively homogeneous in size, ranging from 10–15 nm.

A key aspect of this research was the application of Artificial Neural Networks (ANNs) to model and predict the dielectric strength of the epoxy/BST nanocomposites. The feedforward neural network architecture, with two hidden layers, proved to be highly effective. The ANN models demonstrated excellent accuracy in predicting dielectric strength for both sets of experiments: varying temperature and filler concentration, and varying time and filler concentration. The consistently low percentage errors (below 0.9%) and very low overall mean squared errors (0.000012 for time/filler concentration and 0.000009 for temperature/filler concentration) underscore the reliability and robustness of the developed ANN models. This predictive capability is crucial for optimizing the fabrication process of BST/polymer composites.

The results contribute significantly to understanding the complex interplay between material composition and processing parameters on the dielectric properties of these composites, offering valuable insights for their development in various engineering applications. The proposed theoretical model for dielectric tunability based on the results further enhances the predictive capabilities for future work.

Consenting to the publication of Declarations: not applicable

Ethics and Consenting of the participation of Declarations : not applicable

Author contribution

All Authors have contributed substantially to each step of manuscript preparation and work procedure. In detail, G.M. Rashwan and Mahmoud Rihan said: the idea of the manuscript; G.M. Rashwan, Abdelhameid Ghazzaly and Massaud Mostafa said: conceptualization and methodology. G.M. Rashwan, Loai S. Nasrat and Massaud Mostafa: formal analysis. All authors contributed to the article writing, reviewing, and editing and approved the submitted version.

Funding statement

This research did not receive any specific grant from funding agencies in the public, commercial, or not-for-profit sectors.

Data availability

The datasets used and/or analyzed during the current study are available from the corresponding author on reasonable request.

Competing interest

The authors declare no conflict of interest.

Guidelines and Legislation.

The authors declare that this study was in accordance with relevant institutional, national, and international guidelines and legislation.

References

[1] G. S. Divya and B. Suresha, *Impact of Nano-Silicon Dioxide on Mechanical Properties of Carbon Fabric Reinforced Epoxy Composites*, Mater. Today Proc. **46**, 8999 (2021).

[2] D. Hull and T. W. Clyne, *An Introduction to Composite Materials*, 2nd ed. (Cambridge University Press, Cambridge, 1996).

[3] Y. Karabul and O. İçelli, *The Assessment of Usage of Epoxy Based Micro and Nano-Structured Composites Enriched with Bi2O3 and WO3 Particles for Radiation Shielding*, Results Phys. **26**, 104423 (2021).

[4] K. S. Meenakshi and S. A. Kumar, *Development of Siloxane Based Tetraglycidyl Epoxy Nanocomposites for High Performance Applications—Study of the Thermo Mechanical, Electrical, XRD, EDS and Physical Properties*, Silicon **11**, 741 (2019).

[5] K. Shree Meenakshi, E. Pradeep Jaya Sudhan, S. Ananda Kumar, and M. J. Umapathy, *Development and Characterization of Novel DOPO Based Phosphorus Tetraglycidyl Epoxy Nanocomposites for Aerospace Applications*, Prog. Org. Coatings **72**, 402 (2011).

[6] K. Shree Meenakshi, E. Pradeep Jaya Sudhan, and P. G. Menon, *Analysis of Sulphone Based Organic–Inorganic Hybrid Epoxy Nanocomposites for Advanced Engineering Applications—Study of the Mechanical, Thermomechanical, XRD, EDS and Physical Properties*, Mater. Sci. Eng. A **536**, 152 (2012).

[7] R. Narendar and K. Priya Dasan, *Chemical Treatments of Coir Pith: Morphology, Chemical Composition, Thermal and Water Retention Behavior*, Compos. Part B Eng. **56**, 770 (2014).

[8] X. Kornmann, L. A. Berglund, R. Thomann, R. Mulhaupt, and J. Finter, *High Performance Epoxy-Layered Silicate Nanocomposites*, Polym. Eng. Sci. **42**, 1815 (2002).

[9] S. Sugiman, S. Salman, and M. Maryudi, *Effects of Volume Fraction on Water Uptake and Tensile Properties of Epoxy Filled with Inorganic Fillers Having Different Reactivity to Water*, Mater. Today Commun. **24**, 101360 (2020).

[10] M. Frigione and M. Lettieri, *Durability Issues and Challenges for Material Advancements in FRP Employed in the Construction Industry*, Polymers.

[11] A. S. R., R. P. K., S. N. R., and A. Mart, *Thermal Properties of Biopolymers BT - Handbook of Biopolymers*, in edited by S. Thomas, A. AR, C. Jose Chirayil, and B. Thomas (Springer Nature Singapore, Singapore, 2022), pp. 1–28.

[12] S. Raghavendra, R. R. Sannegowda, A. K. Rudrappa, and S. K. K. Basavarajaiah, *Enhancement of Tensile Strength and Fracture Toughness Characteristics of Banana Fibre Reinforced Epoxy Composites with Nano MgO Fillers*, Next Mater. **5**, 100258 (2024).

[13] Q. Liu and M. Hughes, *The Fracture Behaviour and Toughness of Woven Flax Fibre Reinforced Epoxy Composites*, Compos. Part A Appl. Sci. Manuf. **39**, 1644 (2008).

[14] C. Zhu, Z. Cai, X. Cao, Z. Fu, L. Li, and X. Wang, *High-Dielectric-Constant Nanograin BaTiO3-Based Ceramics for Ultra-Thin Layer Multilayer Ceramic Capacitors via Grain Grading Engineering*, Adv. Powder Mater. **1**, 100029 (2022).

[15] D. Xu, W. L. Li, L. D. Wang, W. Wang, W. P. Cao, and W. D. Fei, *Large Piezoelectric Properties Induced by Doping Ionic Pairs in BaTiO3 Ceramics*, Acta Mater. **79**, 84 (2014).

[16] V. Paunovic, V. V Mitic, and L. Kocic, *Dielectric Characteristics of Donor-Acceptor Modified BaTiO3 Ceramics*, Ceram. Int. **42**, 11692 (2016).

[17] S. Lahiry and A. Mansingh, *Dielectric Properties of Sol–Gel Derived Barium Strontium Titanate Thin Films*, Thin Solid Films **516**, 1656 (2008).

[18] M. Tihtih, J. F. M. Ibrahim, E. Kurovics, and M. Abdelfattah, *Study on the Effect of Bi Dopant on the Structural and Optical Properties of BaTiO3 Nanoceramics Synthesized via Sol-Gel Method*, J. Phys. Conf. Ser. **1527**, 12043 (2020).

[19] Y. LeCun, Y. Bengio, and G. Hinton, *Deep Learning*, Nature **521**, 436 (2015).

[20] J. Schmidhuber, *Deep Learning in Neural Networks: An Overview*, CoRR **abs/1404.7**, (2014).

[21] L. Deng and D. Yu, *Deep Learning: Methods and Applications* (now, 2014).

[22] L. Alzubaidi, J. Zhang, A. J. Humaidi, A. Al-Dujaili, Y. Duan, O. Al-Shamma, J. Santamaría, M. A. Fadhel, M. Al-Amidie, and L. Farhan, *Review of Deep Learning: Concepts, CNN Architectures, Challenges, Applications, Future Directions*, J. Big Data **8**, 53 (2021).

[23] I. Goodfellow, Y. Bengio, and A. Courville, *Deep Learning* (MIT Press, 2016).

[24] A. Shrestha and A. Mahmood, *Review of Deep Learning Algorithms and Architectures*, IEEE Access **7**, 53040 (2019).

[25] *Sejnowski-the-Unreasonable-Effectiveness-of-Deep-Learning-in-Artificial-Intelligence.Pdf*.

[26] M. E. Azim Araghi, N. Shaban, and M. Bahar, *Synthesis and Characterization of Nanocrystalline Barium Strontium Titanate Powder by a Modified Sol-Gel Processing*, Mater. Sci. **34**, 63 (2016).

[27] X. Lyu, H. Wang, Z. Guo, and Z. Peng, *Dielectric Properties of Epoxy-Al2O3 Nanocomposites*, in *2016 IEEE International Conference on Dielectrics (ICD)*, Vol. 2 (2016), pp. 1081–1084.

[28] Z. Guo, H. Wang, H. Li, C. Wang, X. Lv, and Z. Peng, *Experiment Study on Arc Ablation Resistance Performance of Epoxy with Alumina Fillers*, in *2015 IEEE 11th International Conference on the Properties and Applications of Dielectric Materials (ICPADM)* (2015), pp. 620–623.

[29] T. J. Sejnowski, *The Unreasonable Effectiveness of Deep Learning in Artificial Intelligence*, Proc. Natl. Acad. Sci. **117**, 30033 (2020).

[30] O. Vryonis, D. L. Anastassopoulos, A. A. Vradis, and G. C. Psarras, *Dielectric Response and Molecular Dynamics in Epoxy-BaSrTiO3 Nanocomposites: Effect of Nanofiller Loading*, Polymer (Guildf). **95**, 82 (2016).

[31] M. Mostafa, K. Ebnalwaled, H. A. Saied, and R. Roshdy, *Effect of Laser Beam on Structural, Optical, and Electrical Properties of BaTiO3 Nanoparticles during Sol-Gel Preparation*, J. Korean Ceram. Soc. **55**, 581 (2018).

[32] K. Momma and F. Izumi, *{\it VESTA3} for Three-Dimensional Visualization of Crystal, Volumetric and Morphology Data*, J. Appl. Crystallogr. **44**, 1272 (2011).

[33] S. Rahimi, O. Jahanbakhsh, and I. Ahadzadeh, *Effects of Pb2O3 Nanoparticles on Thermal and Mechanical Properties of Epoxy Resin, Silicone, and PVC-Based Nanoshields*, Prog. Nucl. Energy **169**, 105083 (2024).

[34] M. Thakran and S. Lata, *Polybenzopyrrole/Nano-Alumina Composite Blend with Zirconium Silicate Reinforced Epoxy as Protective Coating to Subside Corrosion of Carbon Steel within a Dilute NaCl Solution*, J. Mol. Struct. **1298**, 137068 (2024).

[35] M. Zhang, P. Xu, H. Peng, and F. Qin, *A Rational Design of Core-Shell-Satellite Structured BaTiO3 Fillers for Epoxy-Based Composites with Enhanced Microwave Dielectric Constant and Low Loss*, Compos. Part B Eng. **215**, 108764 (2021).

[36] Y. Zhou, J. Zhang, R. Zhang, E. Liu, X. Xue, X. Xing, and Q. Zhang, *Effect of Nano-Al2O3/Epoxy Resin Composite on the Shear Strength Recovery of Fractured Rock Masses with Various Crack Widths and SCA Interfacial Treatments*, Case Stud. Constr. Mater. **18**, e01715 (2023).

[37] Y. Li, X. Liu, J. Yuan, and M. Wu, *Toughness Improvement of Epoxy Resin Mortar by Incorporation of Ground Calcium Carbonate*, Constr. Build. Mater. **100**, 122 (2015).